THE JOURNAL OF BIOLOGICAL CHEMISTRY VOL. 290, NO. 9, pp. 5621–5634, February 27, 2015

Correlating Structural and Energetic Changes in Glycine Receptor Activation*

Received for publication, October 2, 2014, and in revised form, December 27, 2014 Published, JBC Papers in Press, January 8, 2015, DOI 10.1074/jbc.M114.616573

Suzanne Scott[‡], **Joseph W. Lynch**[‡§], **and Angelo Keramidas**[‡1]

From the [‡]*Queensland Brain Institute and the* [§]*School of Biomedical Sciences, University of Queensland, Brisbane, Queensland, Australia 4072*

Background: Interactions between $Gln^{-26'}$ (in M1 domain), $Arg^{19'}$ (in M2 domain), and $Lys^{24'}$ (in M2-M3 linker) may reveal molecular mechanisms of glycine receptor activation.
Results: $\alpha1^{Q-26'E}$-containing receptors have longer active periods and lower conductances.
Conclusion: The energy for activation is distributed broadly at the transduction zone.
Significance: These energetic interactions are likely present in multiple pentameric ligand-gated ion channels.

Pentameric ligand-gated ion channels (pLGICs) mediate fast chemoelectrical transduction in the nervous system. The mechanism by which the energy of ligand binding leads to current-conducting receptors is poorly understood and may vary among family members. We addressed these questions by correlating the structural and energetic mechanisms by which a naturally occurring M1 domain mutation ($\alpha1^{Q-26'E}$) enhances receptor activation in homo- and heteromeric glycine receptors. We systematically altered the charge of spatially clustered residues at positions 19′ and 24′, in the M2 and M2-M3 linker domains, respectively, which are known to be critical to efficient receptor activation, on a background of $\alpha1^{Q-26'E}$. Changes in the durations of single receptor activations (clusters) and conductance were used to determine interaction coupling energies, which we correlated with conformational displacements as measured in pLGIC crystal structures. Presence of the $\alpha1^{Q-26'E}$ enhanced cluster durations and reduced channel conductance in homo- and heteromeric receptors. Strong coupling between $\alpha1^{-26'}$ and $\alpha1^{19'}$ across the subunit interface suggests an important role in receptor activation. A lack of coupling between $\alpha1^{-26'}$ and $\alpha1^{24'}$ implies that 24′ mutations disrupt activation via other interactions. A similar lack of energetic coupling between $\alpha1^{-26'}$ and reciprocal mutations in the β subunit suggests that this subunit remains relatively static during receptor activation. However, the channel effects of $\alpha1^{Q-26'E}$ on $\alpha1\beta$ receptors suggests at least one $\alpha1$-$\alpha1$ interface per pentamer. The coupling-energy change between $\alpha1^{-26'}$ and $\alpha1^{19'}$ correlates with a local structural rearrangement essential for pLGIC activation, implying it comprises a key energetic pathway in activating glycine receptors and other pLGICs.

The glycine receptor channel (GlyR)[2] is an anion-selective member of the pentameric ligand-gated ion-channel (pLGIC) family. pLGICs are comprised of modular domains (Fig. 1*A*). The ligand binding pockets are found in the extracellular domain, at subunit interfaces, whereas the permeation gate is located at the transmembrane domain (TD). Between the ligand binding pockets and the gate lies a transduction zone (TZ), made of interacting loops that originate from the extracellular domain, such as loops 2 and 7, and the TD, such as the M2-M3 linker (Fig. 1*A*, *inset*). Channel activation proceeds as a wave-like progression of structural rearrangements, initiated by the ligand binding reaction (1, 2) and conveyed to the gate via interactions across the TZ (3–5).

Structure-function studies of the GlyR, and indeed other pLGICs, have benefitted greatly from the study of naturally occurring mutations that perturb channel activation. These perturbations give rise to impaired neurotransmission at glycinergic synapses, resulting in movement disorders such as hyperekplexia (6). Mutations in the $\alpha1$ subunit have been most informative in this respect (7). Although this subunit readily forms homomeric receptors, synaptic GlyRs mainly comprise heteromers of $\alpha1$ and β subunits (8).

Three hyperekplexia-causing point mutations in the $\alpha1$ subunit TZ are vital for efficient signal transduction. Two of these produce impaired receptor activation; $\alpha1^{R271Q}$ ($\alpha1^{R19'Q}$), which is situated at the extracellular end of M2, and $\alpha1^{K276E}$ ($\alpha1^{K24'E}$) in the M2-M3 linker (Fig. 1*A*). The $\alpha1^{R19'Q}$ mutation gives rise to a reduced single channel conductance and a marked decrease in glycine sensitivity when expressed as homomeric receptors (9, 10). Similarly, the $\alpha1^{K24'E}$ mutation reduces glycine sensitivity in both homo- and heteromeric GlyRs, although no change in single channel conductance was reported (5, 11, 12). A recently identified third mutation, $\alpha1^{Q226E}$ ($\alpha1^{Q-26'E}$), located near the top of M1, gives rise to spontaneous channel opening, a reduction in single channel conductance, but no significant change in whole cell agonist sensitivity (13).

Recently published crystal structures of prokaryotic and eukaryotic pLGIC homologues (14–21) reveal close proximity

* This work was supported by the National Health and Medical Research Council of Australia and Australian Research Council Grant DP 1030101702.
[1] To whom correspondence should be addressed. Tel.: 617-3346-3330; Fax: 617-3346-6301; E-mail: a.keramidas@uq.edu.au.
[2] The abbreviations used are: GlyR, glycine receptor; $GABA_AR$, GABA type-A receptor; GluCl, glutamate-gated chloride channel; pLGIC, pentameric ligand-gated ion channel; TM, transmembrane; TD, transmembrane domain; TZ, transduction zone; MOC, main open exponential component; POPC, 1-palmitoyl-2-oleoyl-*sn*-glycero-3-phosphocholine.

of residues at 19′, 24′, and −26′. A high degree of sequence conservation is also evident at these positions, especially among anion-selective pLGICs, suggesting a common functional relevance. In particular, the $Gln^{-26'}$ side group from one subunit lies in close apposition to $Arg^{19'}$ and $Lys^{24'}$ in the adjacent subunit (Fig. 1*A*, *inset*). Given this proximity, and the observation that all three hyperekplexia-causing mutations involve a potential alteration in charge, it is reasonable to postulate that this discrete TZ subregion constitutes a functional unit with a key role in receptor activation. The recent demonstration, based on whole-cell measurements of $\alpha1^{Q-26'E}$ homomeric GlyRs, that a glutamic acid occupying position −26′ interacts with the arginine at 19′ during channel activation (22), supports this idea.

With the exception of $\alpha1^{K24'E}$-containing receptors, investigations into the effects of mutations at the 19′, 24′, and −26′ positions have mainly been confined to homomeric receptors examined via whole cell patch clamp analysis. This affords only limited mechanistic insights into the channel activation mechanism and, of course, avoids the physiologically relevant $\alpha1\beta$ GlyR isoform.

To address these deficiencies we conducted a single channel study that examines the effects of charge-altering mutations to 19′, 24′ in the $\alpha1$ and β subunits, co-expressed on a background of the newly described $\alpha1^{Q-26'E}$ mutation. We employed two key functional parameters of single channel currents to infer the presence of charge and residue interactions. The first of these was the main unitary conductance state of the channel, which was taken as an index of net charge strength near the central conduction pathway (23, 24). The second parameter was the mean duration that a receptor remains active for (cluster duration) in the presence of agonist. These parameters were used alone or in combination to quantitate the strength of interactions between the 19′, 24′, and −26′ positions in both homomers and heteromers. Our data suggest that receptor activation involves multiple energetic pathways at the TZ.

EXPERIMENTAL PROCEDURES

Cell Culture—HEK AD293 cells were seeded onto poly-D-lysine-coated glass coverslips and transfected with cDNAs encoding human $\alpha1$ (pCIS) and β (pcDNA 3.1+) GlyR subunits using a calcium phosphate-DNA co-precipitate method. The cDNA encoding the CD4 surface antigen was also added to the transfection mixture and acted as a marker of transfected cells. For some transfections, empty (non-coding) pCIS cDNA plasmid was included to reduce expression levels and facilitate the resolution of single-channel activations (25). To minimize the formation of homomeric receptors, heteromeric GlyRs were expressed by cotransfecting the $\alpha1$ and β cDNAs at an $\alpha1$:β ratio of 1:100. We will provisionally assume a stoichiometry and subunit arrangement of β-$\alpha1$-β-$\alpha1$-β (26, 27) but will consider other possibilities, see "Discussion." Cells were used in experiments 2–3 days after transfection. Point mutations were incorporated into the subunits using the QuikChange site-directed mutagenesis method. The homomeric $\alpha1^{K24'C}$ cross-linking experiments were done on an $\alpha1^{C41A}$ background. Successful incorporation of mutations was confirmed by sequencing the mutated DNA.

Electrophysiology—All experiments were carried out at room temperature (21–24 °C). Single-channel and macropatch currents were recorded from outside-out excised patches at a clamped potential of −70 mV, unless indicated otherwise. The cells were continuously perfused via a gravity-fed plastic tube with an extracellular bath solution containing (in mM), 140 NaCl, 5 KCl, 1 $MgCl_2$, 2 $CaCl_2$, 10 HEPES, and 10 D-glucose and titrated to pH 7.4. Glass electrodes were pulled from borosilicate glass (G150F-3; Warner Instruments), coated with a silicone elastomer (Sylgard-184; Dow Corning), and heat-polished to a final tip resistance of 4–15 MΩ when filled with an intracellular solution containing (in mM) 145 CsCl, 2 $MgCl_2$, 2 $CaCl_2$, 10 HEPES, and 5 EGTA, pH 7.4. Excised patches were directly perfused with extracellular solution by placing them in front of one barrel of a double-barreled glass tube. Single channel currents were elicited by exposing the patch continuously to glycine containing solution, flowing through the adjacent barrel, by lateral switching of the tube. Experiments were recorded using an Axopatch 200B amplifier (Molecular Devices), filtered at 5 kHz (2 kHz for the $\alpha1^{Q-26'E/R19'A}$ double mutant) and digitized at 20 (ensemble currents) or 50 kHz (single-channel currents) using Clampex (pClamp 10 suite, Molecular Devices) via a Digidata 1440A digitizer.

Data Analysis—Single-channel current amplitudes were measured in Clampfit. The current amplitude of most receptors was estimated using amplitude histograms. However, for receptors that produced activations containing many unresolved openings (see Fig. 3*A*) we opted for direct cursor measurement of expanded sections of record that showed fully resolved levels. Multiple measurements of openings of the largest amplitude were made from at least three patches for each channel type held at −70 mV. In current-voltage (*i-V*) experiments, the amplitude was measured at voltages of ±70, ±35, ±15, and 0 mV. The data were fit to a polynomial function in SigmaPlot (Systat Software) and the reversal potential was read directly off the plots. Single-channel conductance (γ) was calculated from the single-channel amplitude (i) using Ohm's law,

$$\gamma = \frac{i}{V_{hold} - V_{ljp} - V_{rev}} \qquad \text{(Eq. 1)}$$

where V_{hold} is the holding potential (−70 mV), V_{ljp} is the liquid junction potential, and V_{rev} is the reversal potential. V_{ljp} was calculated to be 4.7 mV for the solutions used (28). We confined our analysis to the largest, main conductance level.

The QuB suite was used to analyze the kinetic properties of GlyR activations. Segments of single-channel activity separated by long periods of baseline were selected by eye and idealized into noise-free open and shut events using a temporal resolution of 70 μs (29). Idealized data were fit with a simple model in which open and shut states were connected to a central shut state. Rate constants for transitions in the model were optimized using Maximum Likelihood Fitting (30), and states were added, to the central shut state, and re-fit until the log likelihood improved by less than 10 units. This fit was used to determine the critical time (t_{crit}), which was taken for the shut durations and used to divide the idealized segments into clusters (or bursts at 2 μM glycine). t_{crit} varied between 9 and 51 ms and

generally preserved three shut components when the divided (chopped) data were re-fit in the manner described above. This analysis yielded mean cluster durations, intra-cluster open probabilities (P_o), and number of events per cluster. In addition, we monitored the effects of the mutations on the time constant of the main open exponential component (MOC) in the open dwell histograms of the re-fitted data. The MOC accounted for 51–96% of the current.

We used cluster duration and conductance to assay channel function. Cluster duration is a function of the net affect of all the equilibrium constants in the underlying activation mechanism and, as such, is an integrated index of the entire activation process. A point mutation will affect multiple state transitions along the activation coordinate, and it is experimentally intractable to determine which state-to-state transitions mutations will be affected. Because it is not possible to know, *a priori*, what the physical correlate of a particular equilibrium constant is, we avoided using any particular equilibrium constant as an index of receptor function, including in the pairwise interaction energy calculations.

Any mutation-induced change in conductance was taken to indicate that a given residue is charged. The magnitude of the change in conductance reflects the strength of the charge. Because we are only interested in factors affecting the activation process, we made no inferences regarding the determinants of permeation to avoid conflating the processes of activation and ion permeation. We used cluster duration and conductance as measures of the electrostatic topography of the gating landscape, exploiting the fact that the region of interest happens to be near the permeation pathway, thus giving us a measurable way of ascertaining the effective charge of relevant residues. As a measure of open state stability we monitored the shutting frequency within active periods. This proved to be a more sensitive stand-alone parameter than more conventional ones, such as intracluster P_o. P_o was only used in conjunction with cluster duration as an alternative method of calculating coupling energies.

Parameter measurements were plotted in Prism 6 (GraphPad). Data were analyzed by ordinary one-way analysis of variance in Prism, and Sidak's multiple comparisons test was used in the case of significance. Because cluster and burst durations, MOCs, and shutting frequencies are exponentially distributed, we analyzed these data on a patch-to-patch basis. Mean values for cluster duration, MOC, and shutting frequency were determined for each patch for a given receptor (these are normally distributed). Analysis of variance tests were applied to these means. The overall mean was then determined for plotting and data interpretation. Statistical significance was set at $p < 0.01$, and all data are presented as mean ± S.E.

Cluster (or burst) durations were determined for the largest conductance level for each receptor. The energy of interaction between two residue positions incorporating mutations in the receptors was determined using,

$$\Delta\Delta G_{\text{int}} = -RT \ln\left(\frac{\Theta_{wt}\Theta_{dm}}{\Theta_{sm1}\Theta_{sm2}}\right) \quad \text{(Eq. 2)}$$

where $\Delta\Delta G_{\text{int}}$ is the first-order coupling free energy (in kJ mol^{-1}) in a mutant cycle, R is the gas constant, T is absolute temperature, and Θ is the product of the channel conductance and cluster duration at saturating concentrations of glycine for wild-type (wt), double mutant (dm), single mutant 1 (sm1), and single mutant 2 (sm2). Alternative parameters for Θ are shown in Table 2.

Ensemble currents were recorded in response to brief (<1 ms) exposure to a saturating concentration of glycine by rapidly moving the double-barreled tube by means of a piezoelectric translator (Siskyou MXPZT-300), controlled by a voltage-step protocol in Clampex. The exchange time (rise and decay ~200 μs) was verified for each recording session by monitoring changes in the liquid junction potential using an open-tip electrode. Ten to fifteen responses from each patch were peak-normalized and averaged. The rise and decay times constants were measured by fitting 10–100% of the rising phase of the current to,

$$I(t) = A(1 - e^{-t/\tau}) + C \quad \text{(Eq. 3)}$$

and the 20–80% of the decay phase of the current using,

$$I(t) = \sum_{j=1}^{n} A_j e^{-t/\tau} + C \quad \text{(Eq. 4)}$$

where A is the amplitude, t is time, τ is the time constant, and C is a constant. The number of components (j) ranged from one to three to give the best fit as determined by eye. To facilitate comparison between the decay time constants, the weighted average time constant (τ_w) was calculated using the following equation.

$$\tau_w = \frac{\sum_{j=1}^{n} A_j \tau_j}{\sum_{j=1}^{n} A_j} \quad \text{(Eq. 5)}$$

RESULTS

Current-Voltage (i-V) Plots and Conductance—Our first experiments were aimed at accurately calculating the conductance of each receptor at −70 mV. Single channel current amplitude was measured over a voltage range of ±70 mV for three GlyRs to establish if the reversal potential varied between receptors incorporating a change of charge near the extracellular pore entrance. We tested the homomeric α1 wild-type, $\alpha1^{Q-26'E}$, and $\alpha1^{R19'Q}$ receptors, the latter two involving a potential alteration in charge near the pore lumen. The largest, predominant current level was considered for α1 wild-type and $\alpha1^{Q-26'E}$ receptors, elicited by glycine concentrations of 20 μM (α1 wild-type) and 1 μM ($\alpha1^{Q-26'E}$) (Fig. 1*B*, Table 1). Previous reports suggest that the homomeric $\alpha1^{R19'Q}$ GlyR exhibits either a single conductance of 18 pS (10) or two conductances, with one being predominant (15 pS, >99%) and the other being rare (37 pS, <1%) (9). We found that $\alpha1^{R19'Q}$ receptors exhibited multiple levels when exposed to glycine concentrations from 2 to 300 mM. We analyzed the smallest and largest of these levels (Fig. 1*C*). The *i-V* for all three channels intersected the voltage axis at 4.0 mV (Fig. 1*D*), allowing us to correct for the driving force according to Equation 1. The corresponding conductance calculations yielded values of 92.5 ± 0.3 pS for α1 wild-type and 60.6 ± 0.4 pS for $\alpha1^{Q-26'E}$ receptors. For the $\alpha1^{R19'Q}$ receptors the conductance values were 14.9 ± 0.5 and

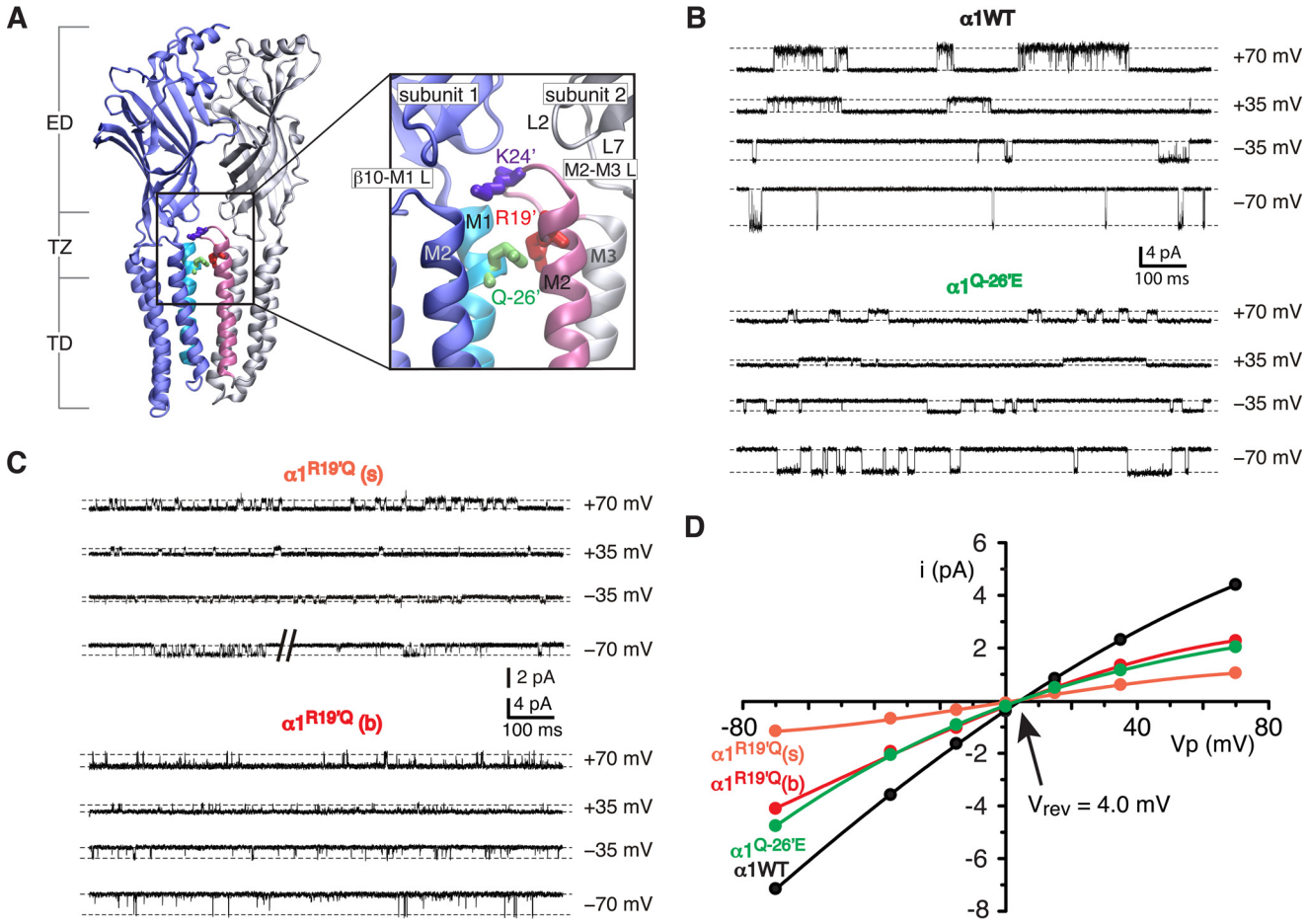

FIGURE 1. ***i-V* and conductance.** *A,* schematic representation of two adjacent subunits showing the extracellular domain (*ED*), TZ, and TD. The *inset* shows an expanded view of the TZ (*boxed*) and residues Lys$^{24'}$ (Lys^{276}), Arg$^{19'}$ (Arg^{271}), and Gln$^{-26'}$ (Gln^{226}). The schematic is based on the β3 GABA$_A$ receptor (Protein Data Bank code 4COF) (21). *B,* sample currents obtained at ±70 and ±35 mV for homomeric α1 wild-type and α1$^{Q-26'E}$ receptors. *C,* sample currents obtained at ±70 and ±35 mV for the smallest (R19′Q(s)) and largest (R19′Q(b)) current amplitudes of α1$^{R19'Q}$ homomeric receptors. *D,* group *i-V* for the experiments shown in *B* and *C*. The number of patches used for the *i-V* was 10 (wild-type), 11 (Q−26′E), 11 (R19′Q(s)), and 6 (R19′Q(b)).

TABLE 1
GlyRs used in this study

	α1 Homomers	α1β Heteromers
Wild-type	α1	α1β
Mutants	α1$^{Q-26'E}$	α1$^{Q-26'E}$β
	α1$^{R19'Q}$	
	α1$^{R19'A}$	α1β$^{A19'R}$
	α1$^{K24'C}$	
	α1$^{K24'A}$	α1β$^{K24'A}$
	α1$^{Q-26'E/R19'A}$	α1$^{Q-26'E}$-β$^{A19'R}$
	α1$^{Q-26'E/K24'A}$	α1$^{Q-26'E}$-β$^{K24'A}$

52.7 ± 0.8 pS for the small and large amplitude currents, respectively. As all four plots reversed current at 4.0 mV, irrespective of the receptor type or conductance level measured, we infer that mutations at the subregion under investigation do not affect the reversal potential. For calculations of conductance for other receptors we will assume that they too reverse current at 4.0 mV.

Wild-type and α1$^{Q-26'E}$ Homo- and Heteromeric GlyRs—Having established an accurate method for calculating channel conductance, we compared single channel currents recorded from homomeric α1 wild-type and α1$^{Q-26'E}$ receptors, with those of the same receptors incorporating the β subunit (Table 1). As previously noted, wild-type homo- and heteromeric receptors exhibit negligible spontaneous (agonist-free) activations (12, 31)(Fig. 2*A*, *above*). At a saturating (1 mM) glycine concentration, active periods occurred as clusters of openings flanked by quiet periods that correspond to receptor desensitization (Fig. 2*A*, *below*). We also observed spontaneous channel activity in α1$^{Q-26'E}$ homomeric receptors (Fig. 2*B* *above*), as previously reported (13). As evidence was adduced for an interaction between the introduced glutamic acid at −26′ in one subunit and the Arg$^{19'}$ position in the adjacent subunit (22) we investigated the effect of introducing the wild-type β subunit, which has an alanine at 19′. To our surprise, α1$^{Q-26'E}$-β heteromers were also constitutively active (Fig. 2*B*, *above*). This suggests that there might be additional residues that can interact with α1$^{Q-26'E}$ in α1 and β subunits that give rise to spontaneous openings, or that at least one α1-α1 interface exists in α1β heteromeric receptors.

Channel conductance, cluster durations, the MOC, and the shutting frequency within each cluster were determined for the four receptors (Fig. 2*C*). Consistent with previous reports (12, 32, 33), the main conductance for wild-type homo- and heteromeric receptors was 92.5 ± 0.3 and 45.9 ± 1.4 pS, respectively. The mean cluster duration for wild-type α1 receptors was 1175 ± 246 ms and for α1β receptors was 466 ± 60 ms. The

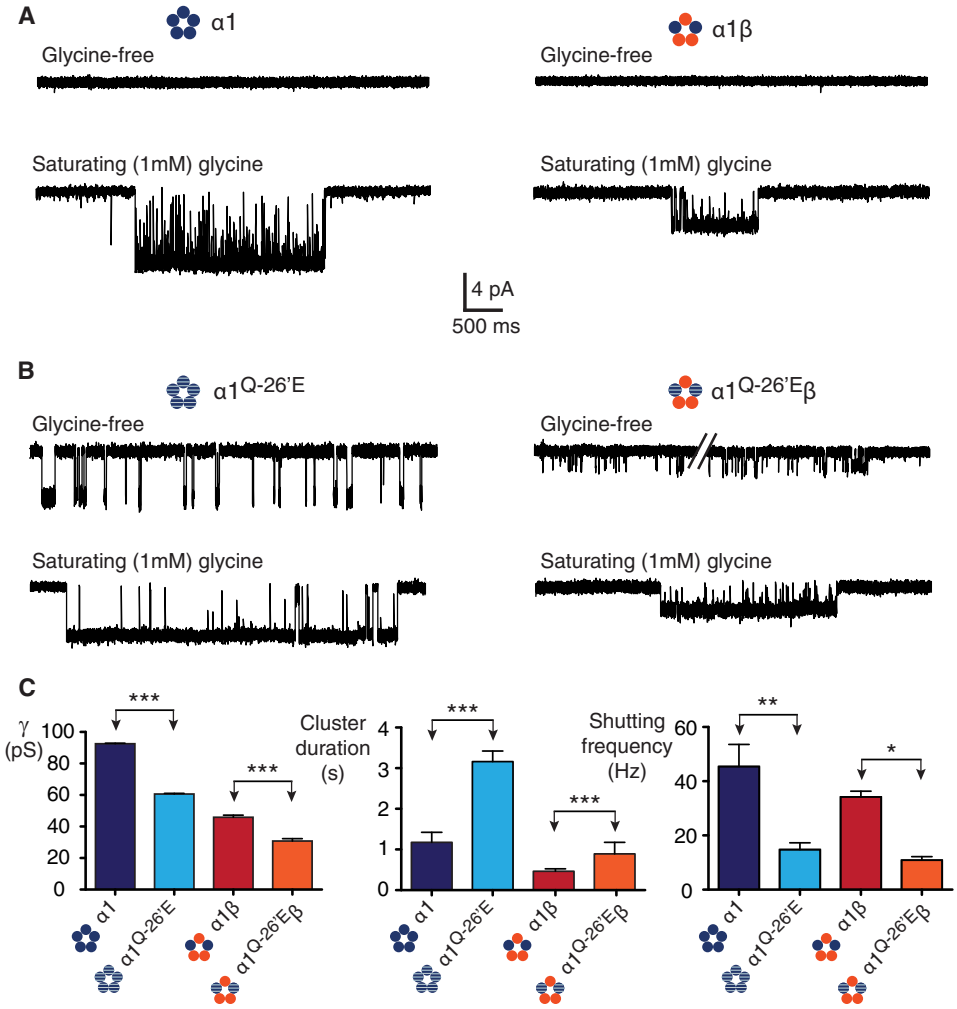

FIGURE 2. **Constitutive activity in $\alpha1^{Q-26'E}$-containing homo- and heteromeric GlyRs.** *A*, wild-type $\alpha1$ homo- and $\alpha1\beta$ heteromeric receptors show no significant spontaneous activity in glycine-free solution. In saturating glycine receptor activations occur as clusters of open and shut events that define the activity of a single channel. In this and all subsequent figures, recordings were performed at −70 mV and channel openings are downward deflections. *B*, in the absence of glycine, $\alpha1^{Q-26'E}$ homo- and $\alpha1^{Q-26'E}$-β heteromeric receptors activate in brief bursts. In saturating glycine, $\alpha1^{Q-26'E}$-containing receptors activate in clusters of longer duration, lower conductance, and a reduced intra-cluster shutting frequency compared with their wild-type counterparts. *C*, group data summarizing the effects on channel conductance, cluster duration, and intra-cluster shutting frequency for wild-type and $\alpha1^{Q-26'E}$-containing receptors. The number of clusters used in the analysis was 175 ($\alpha1$ wild-type, 10 patches), 69 ($\alpha1\beta$ wild-type, 8 patches), 124 ($\alpha1^{Q-26'E}$, 9 patches), and 72 ($\alpha1^{Q-26'E}$-β, 9 patches). ***, $p < 0.0001$; **, $p < 0.001$; *, $p < 0.01$.

shutting frequency within clusters, a measure of open state stability, for $\alpha1$ and $\alpha1\beta$ wild-type receptors was 45 ± 8 and 34 ± 2 Hz, respectively. The corresponding MOCs for $\alpha1$ and $\alpha1\beta$ receptors were 24 ± 6 (fraction 74 ± 4%) and 32 ± 3 ms (fraction 78 ± 6%), with no significant difference between the time constants or fractions.

In homomeric $\alpha1^{Q-26'E}$ receptors, the introduction of a glutamic acid decreased the channel conductance to 60.6 ± 0.4 pS, dramatically increased the mean cluster length to 3161 ± 262 ms, and decreased the intracluster shutting frequency to 15 ± 3 Hz. A comparable pattern of changes was observed in $\alpha1^{Q-26'E}$-β heteromers. There was a significant decrease in conductance to 30.8 ± 1.5 pS (Fig. 2*C*), which is proportional to the decrease measured in the homomeric receptors. The mean cluster duration for $\alpha1^{Q-26'E}\beta$ heteromers was 893 ± 283 ms, representing a proportional increase relative to the homomeric mutant receptor. The mean frequency of shutting within clusters mediated by $\alpha1^{Q-26'E}$-β heteromers was 11 ± 1 Hz. The changes in cluster duration and the intracluster shut events reached significance when compared with wild-type $\alpha1\beta$ receptors. The MOCs were 258 ± 28 (fraction 82 ± 7%) and 48 ± 7 ms (fraction 77 ± 8%) for the $\alpha1^{Q-26'E}$ and $\alpha1^{Q-26'E}$-β receptors, respectively. The MOC time constant for the $\alpha1^{Q-26'E}$ homomeric receptors was significantly different from both the wild-type and $\alpha1^{Q-26'E}$-β receptors ($p < 0.0001$).

We infer that the $\alpha1^{Q-26'E}$ mutation confers four effects on GlyRs. First, receptors bearing this mutation are constitutively active. Second, the decrease in conductance demonstrates that the introduced glutamic acid side group carries a negative charge at pH 7.4, and is close enough to the permeation pathway to influence conductance. Third, the negative charge induces longer duration active periods (and greater MOC time constants) within which the conducting states are more stable. Finally, the β subunit dilutes the effect of the $\alpha1^{Q-26'E}$ mutation on cluster properties, but not on conductance.

19′ Mutations on an $\alpha1^{Q-26'E}$ Background—The above results indicate that $\alpha1^{Q-26'E}$ induces spontaneous openings, but that its effects on ligand-induced cluster duration are reduced when the β subunit is present. This suggests that β subunit residues proximal to $\alpha1^{Q-26'E}$ may account for the attenuation. To investigate this further, we introduced mutations at 19′ in the $\alpha1$ and β subunits (Table 1). As with $\alpha1^{R19'Q}$ receptors, the homomeric $\alpha1^{R19'A}$ receptors, in the presence of a saturating glycine concentration (50 mM) also showed a significantly reduced conductance (75.0 ± 0.8 pS), a marked decrease in cluster duration to 257 ± 54 ms, a marked leftward shift in the MOC (0.7 ± 0.2 ms, 77 ± 9%), and a substantial increase in shutting frequency (395 ± 18 Hz) compared to the homomeric wild-type (Fig. 3, *A* and *C*). Expressing the $\alpha1^{R19'A}$ on an $\alpha1^{Q-26'E}$ background produced the $\alpha1^{Q-26'E/R19'A}$ homomeric receptor. Functional impairment was most severe in this double mutant receptor (Fig. 3*A*). Notably, all spontaneous activity was ablated. Indeed, little activity was observed for these receptors at glycine concentrations below 100 mM. We used 300 mM glycine to induce enough channel activity for analysis. These receptors opened to a conductance of 8.6 ± 0.7 pS, with a mean cluster length of 89 ± 25 ms, an MOC of 1.2 ± 0.2 ms (fraction 83 ± 5%), and a shutting frequency of 292 ± 41 Hz (Fig. 3*C*).

We then investigated the effect of the reciprocal β subunit mutation in $\alpha1\beta^{A19'R}$ GlyRs. When activated by a saturating (1 mM) glycine concentration, this receptor exhibited a small (~7–8 pS) reduction in conductance (53.7 ± 1.5 pS) and no change to cluster duration (511 ± 179 ms), MOC (30 ± 6 ms, 78 ± 14%), or the frequency of shut events (37 ± 4 Hz) relative to wild-type $\alpha1\beta$ receptors (Fig. 3, *B* and *D*). This demonstrates a functional asymmetry between $\alpha1$ and β subunits, in accord with a previous report based on whole cell experiments (34). That is, when an arginine residue occupies all five 19′ positions in the mutant heteromeric receptors, the functional parameters of conductance, cluster duration, and number of shut events within clusters are nearly indistinguishable from wild-type heteromers. This is in stark contrast to the effects of removing the arginine in the $\alpha1$ subunit.

The heteromeric $\alpha1^{Q-26'E}$-$\beta^{A19'R}$ GlyR also exhibited minimal changes relative to $\alpha1^{Q-26'E}$-β receptors. These receptors were constitutively active (Fig. 3*B*) with a conductance of 29.0 ± 1.5 pS. Glycine (1 mM) elicited clusters with a mean duration of 639 ± 106 ms, an MOC of 69 ± 5 ms (fraction 91 ± 6%), and a shutting frequency of 22 ± 2 Hz. The parameters of conductance, cluster duration, and MOC were not significantly different from the $\alpha1^{Q-26'E}$-β receptors (Fig. 3*D*), whereas there was a small but significant difference in shutting frequency. Together, these data demonstrate the significance of the arginine residue at 19′ in the $\alpha1$ subunit on receptor activation, in contrast to the β subunit, where the functional influence of this residue is minimal. The existence of spontaneous activity in $\alpha1^{Q-26'E}$-β and $\alpha1^{Q-26'E}$-$\beta^{A19'R}$ receptors implies the presence of at least one $\alpha1$-$\alpha1$ interface. Alternatively, $\alpha1^{Q-26'E}$ may interact with different residues in $\alpha1$ *versus* β subunits, giving rise to the observed effects.

24′ Mutations on an $\alpha1^{Q-26'E}$ Background—A possible candidate residue that might interact with the $\alpha1^{Q-26'E}$ residue is $Lys^{24'}$. This residue is highly conserved, like $Arg^{19'}$, has a basic side group, and is critical to efficient channel activation in the $\alpha1$ subunit (5, 35), especially when mutated to a hyperekplexia-causing glutamic acid (11, 12). Moreover, $Lys^{24'}$ sits on a segment (the M2-M3 linker) that is mobile enough to permit K24′C cross-linking between $\alpha1$ subunits in functional GlyRs. This mobility was tested on $\alpha1^{K24'C}$ homomeric channels (Fig. 4*A*, Table 1). In the presence of glycine alone, the activations were sporadic and short-lived, as illustrated by the single ~2 ms open dwell-time component (Fig. 4*B*, *left*). Following application of the reducing agent, DTT (4 mM), for a duration of 3–6 min in three patches, the mean burst duration increased dramatically to ~90 ms and the open dwell-time distributions showed multiple components (Fig. 4*B*, *right*). This observation, and the demonstration of H_2O_2-induced reversibility (22) suggests that DTT reduces pre-existing disulfide bonds formed between $\alpha1^{K24'C}$ residues. No significant difference was detected in conductance for this mutant (90.0 ± 0.5 pS) compared with wild-type, either before or after DTT application. We reasoned that the high amplitude movement of the M2-M3 linker during the activation process could bring $Lys^{24'}$ close enough to $\alpha1^{Q-26'E}$ to facilitate interaction between the two. This is also consistent with the pLGIC crystal structures that show proximity between the $Lys^{24'}$ and −26′ positions (Fig. 1*A*).

We tested mutant channels that incorporated the K24′A substitution in $\alpha1$ and β subunits. Representative current traces are shown in Fig. 4, *C* and *D*. The first of these was the $\alpha1^{K24'A}$ homomeric GlyR (Fig. 4*C*). A saturating (50 mM) glycine concentration induced clusters with a conductance of 89.1 ± 1.6 pS, representing a nonsignificant change compared with $\alpha1$ wild-type homomers. Greater differences were observed in the kinetic properties of the receptors. Cluster duration and the MOC were an order of magnitude briefer at 214 ± 23 and 3.0 ± 1 ms (fraction 51 ± 1%), whereas the intracluster shutting frequency was an order of magnitude higher at 324 ± 88 Hz (Fig. 4*E*). The $\alpha1^{K24'A}$ mutation was then combined with the $\alpha1^{Q-26'E}$ to produce the double mutant $\alpha1^{Q-26'E/K24'A}$ homomeric receptor. These were active in the absence of glycine (Fig. 4*C*) and had a similar channel conductance (56.4 ± 1.6 pS) to the $\alpha1^{Q-26'E}$ homomers. Clusters of activity induced by 50 mM glycine had a mean duration of 882 ± 158 ms and the receptor shut at a frequency of 23 ± 3 Hz while active (Fig. 4*F*). The MOC for this receptor was 124 ± 26 ms (fraction 96 ± 3%).

Similar experiments were conducted using the equivalent β subunit mutation ($\beta^{K24'A}$), which was initially expressed with the wild-type $\alpha1$ subunit (Fig. 4*D*). No significant changes were observed in this receptor in terms of conductance (45.8 ± 1.8 pS), the MOC (30 ± 4 ms, 90 ± 3%), or mean cluster duration (390 ± 81 ms) compared with wild-type heteromeric receptors in the presence of saturating (1 mM) glycine. An influence of the $\beta^{K24'A}$ mutation to channel activation was only evident in the increased frequency of shutting, which was 54 ± 6 Hz (Fig. 4*F*). Heteromers containing $\alpha1^{Q-26'E}$ and $\beta^{K24'A}$ subunits opened to a conductance of 28.1 ± 1.7 pS, which was not significantly different from the $\alpha1^{Q-26'E}$-β heteromers. The cluster duration was 929 ± 75 ms and the shutting frequency within clus-

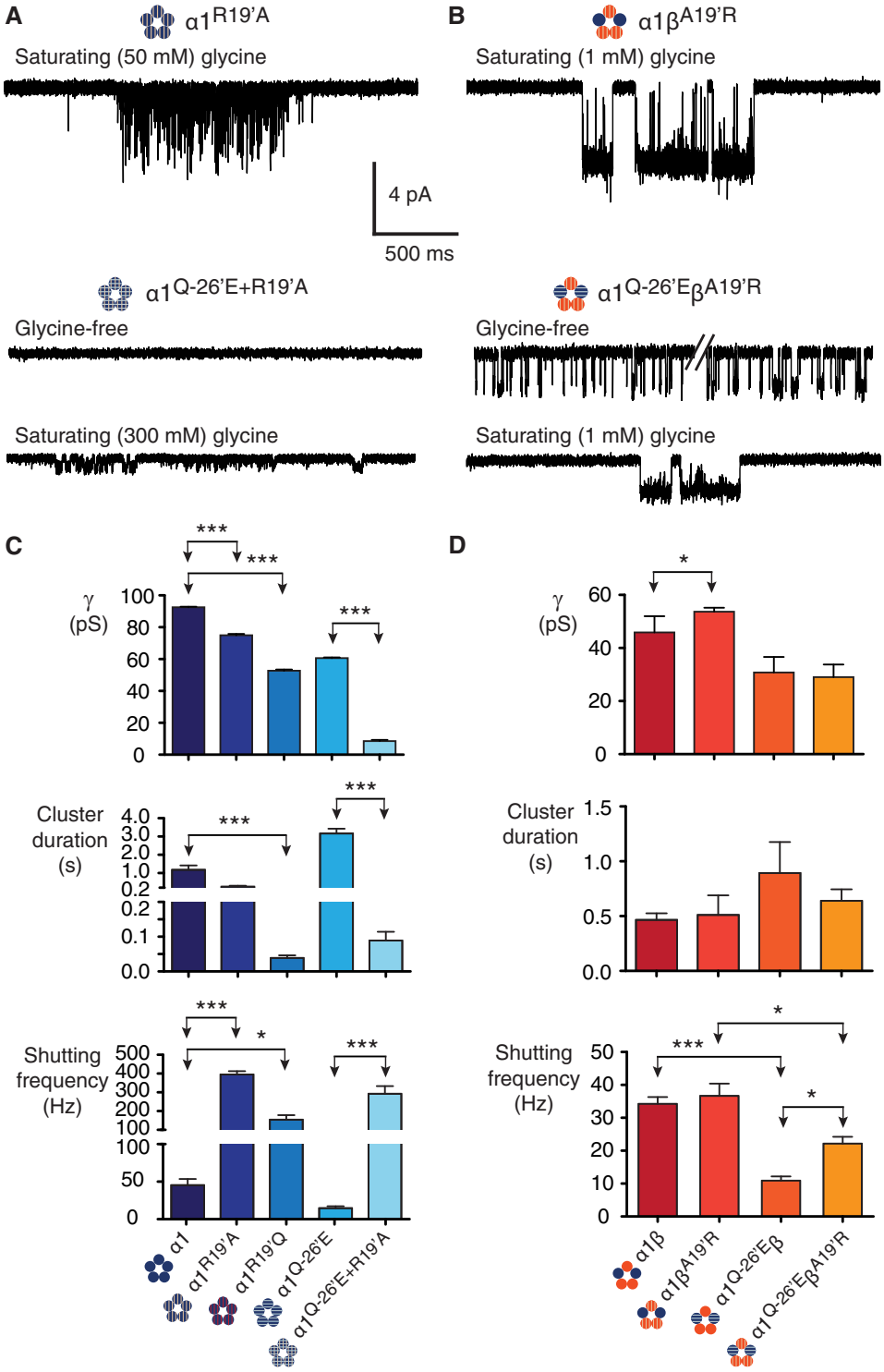

FIGURE 3. **Mutations to 19′.** *A,* homomeric $\alpha1^{R19'A}$ receptors show evidence of impaired receptor activation. When the $\alpha1^{R19'A}$ mutation is combined with the $\alpha1^{Q-26'E}$ mutation in the same subunit ($\alpha1^{R19'A/Q-26'E}$) and expressed as homomers, the functional impairment was greatest, ablating constitutive activity and markedly reducing conductance. *B,* heteromeric receptors containing the $\beta^{A19'R}$ subunit showed little evidence of functional impairment. When expressed with $\alpha1$ wild-type ($\alpha1\beta^{A19'R}$) the receptors had similar properties to wild-type $\alpha1\beta$ heteromers. Similarly, when $\beta^{A19'R}$ was co-expressed with $\alpha1^{Q-26'E}$ the resulting heteromers ($\alpha1^{Q-26'E}$-$\beta^{A19'R}$) were little changed compared with the $\alpha1^{Q-26'E}$-β heteromers. *C,* group data summarizing the effects on channel conductance, cluster duration, and intra-cluster shutting frequency for receptors incorporating 19′ mutations. The number of clusters used in the analysis was 284 ($\alpha1^{R19'A}$, 4 patches), 378 ($\alpha1^{R19'Q}$, 5 patches), 99 ($\alpha1^{Q-26'E/R19'A}$, 10 patches), 35 ($\alpha1\beta^{A19'R}$, 3 patches), and 133 ($\alpha1^{Q-26'E}$-$\beta^{A19'R}$, 5 patches). ***, $p < 0.0001$; *, $p < 0.01$.

ters was 24 ± 2 Hz (Fig. 4*F*). The MOC was 72 ± 17 ms (fraction 92 ± 4%), which was significantly increased compared with the wild-type heteromers ($p < 0.01$), whereas the fraction of the MOC was not. From these data we infer that the effects of the K24′A substitution are smaller than the R19′A substitution in both homomeric and heteromeric receptors. Notably, the

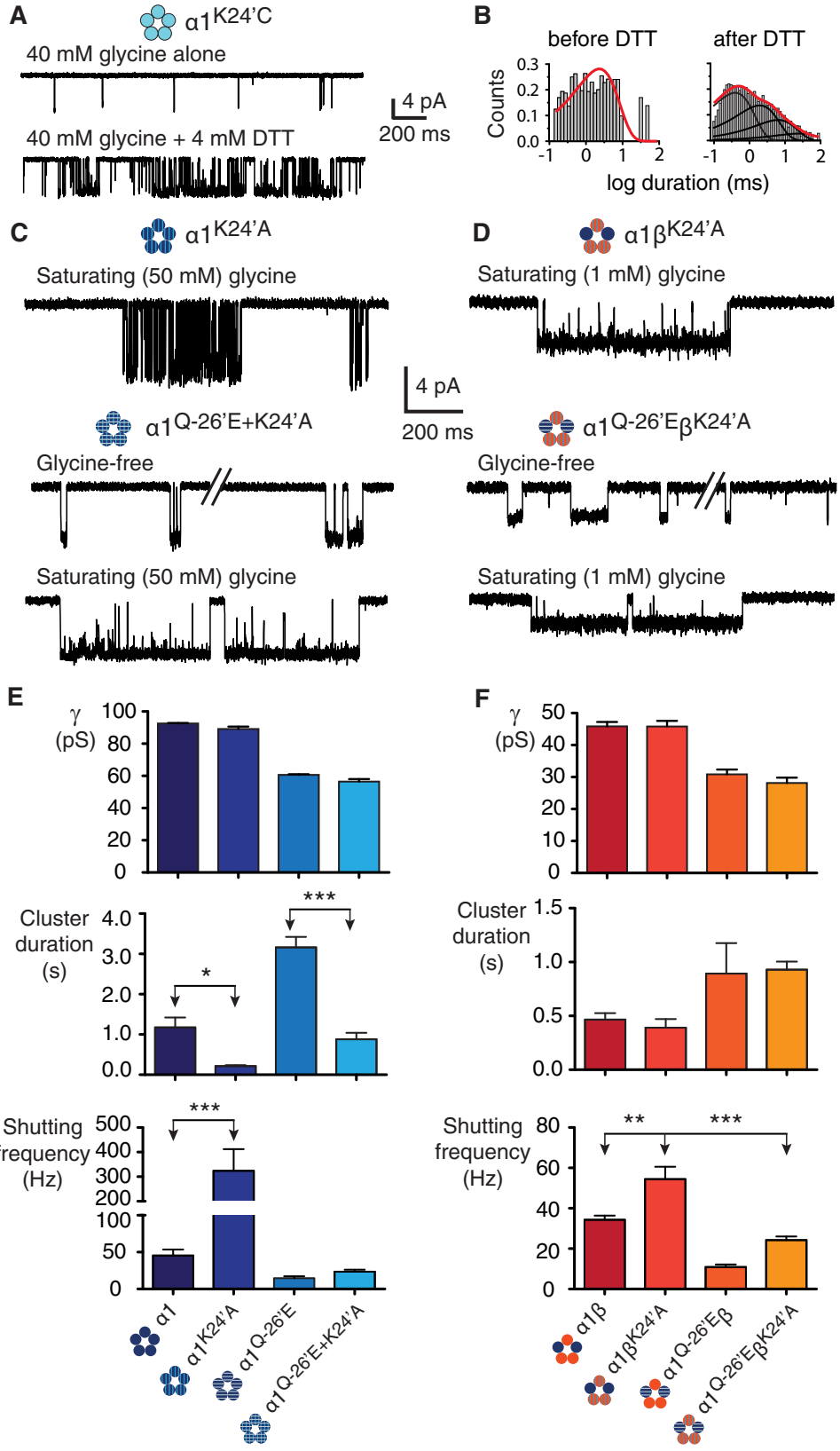
A
α1K24'C
40 mM glycine alone
40 mM glycine + 4 mM DTT
4 pA
200 ms
B
before DTT
after DTT
Counts
log duration (ms)
C
α1K24'A
Saturating (50 mM) glycine
α1Q-26'E+K24'A
Glycine-free
Saturating (50 mM) glycine
D
α1βK24'A
Saturating (1 mM) glycine
α1Q-26'EβK24'A
Glycine-free
Saturating (1 mM) glycine
E
γ (pS)
Cluster duration (s)
Shutting frequency (Hz)
α1
α1K24'A
α1Q-26'E
α1Q-26'E+K24'A
F
γ (pS)
Cluster duration (s)
Shutting frequency (Hz)
α1β
α1βK24'A
α1Q-26'Eβ
α1Q-26'EβK24'A

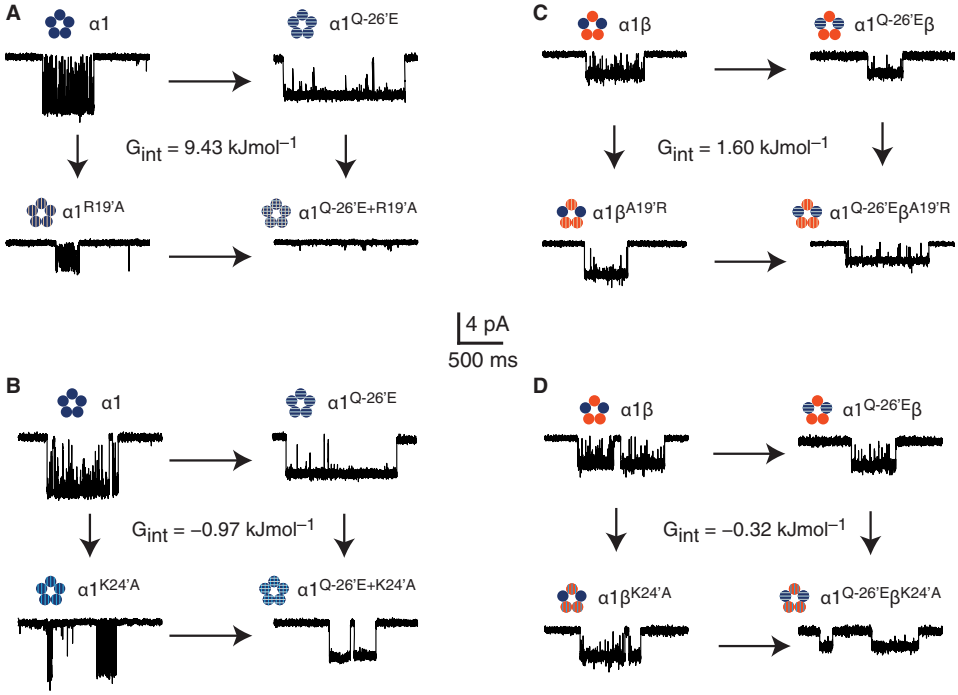

FIGURE 5. **Energetic interactions between −26′ and 19′ or 24′.** Mutant cycle analysis for interactions between −26′ and 19′ (*A*) and the −26′ and 24′ (*B*) in homomeric, and −26′ and 19′ (*C*) and the −26′ and 24′ (*D*) in homomeric GlyRs. Each mutant cycle is accompanied by sample recordings of each receptor and the calculated interaction energy ($\Delta\Delta G_{int}$).

minor effects on channel conductance suggest that whereas the channel is conducting current the $Lys^{24'}$ position is either too far from the permeation pathway to affect conductance or is otherwise neutralized.

The Energetics of $\alpha1^{R19'}$, $\alpha1^{K24'}$, and $\alpha1^{Q-26'E}$ Interactions in Homo- and Heteromeric GlyRs—Our data reveal that $\alpha1^{Q-26'E}$ enhances channel function by conferring spontaneous activity, increasing the time constant of the main open dwell component, lengthening the duration of glycine-induced clusters, and decreasing the transition frequency to shut states while the channel is active. We have assessed the contributions of local electrostatic interactions with 19′ and 24′ residues in both the $\alpha1$ and β subunits in mediating these effects. We next employed channel conductance and cluster duration in an attempt to define the relative strengths of these interactions in the channel activation process. These parameters were used in mutant cycle calculations for four potential interaction partner combinations involving the $\alpha1^{Q-26'E}$ residue (Fig. 5). The first of these was the $\alpha1^{Q-26'}$ and $\alpha1^{R19'}$ cycle. This revealed an interaction energy of 9.43 kJ mol^{-1} (2.3 kcal mol^{-1}) (Fig. 5*A*). The energy of interaction between $\alpha1^{Q-26'}$ and $\alpha1^{K24'}$ was −0.97 kJ mol^{-1} (−0.23 kcal mol^{-1}) (Fig. 5*B*). The coupling energies involving heteromers were lower than for homomeric receptors. The $\alpha1^{Q-26'}$-$\beta^{A19'}$ cycle yielded an interaction energy of 1.60 kJ mol^{-1} (0.38 kcal mol^{-1}) (Fig. 5*C*), whereas the interaction energy for the $\alpha1^{Q-26'}$ and $\beta^{K24'}$ was the lowest, being −0.32 kJ mol^{-1} (−0.08 kcal mol^{-1}) (Fig. 5*D*). Table 2 shows $\Delta\Delta G_{int}$ calculations using other kinetic parameters, in addition to the product of cluster duration and conductance. These include the use of cluster duration and conductance, separately, the product of the cluster duration and open state probability (P_o), and the MOC time constant for each receptor. Overall, these data show that interactions between −26′ and the 19′ and 24′ positions are strongest in $\alpha1$ homomeric receptors, especially the interaction between $\alpha1^{Q-26'}$ and $\alpha1^{R19'}$. Introducing the β subunit, even one bearing an arginine at 19′ did not increase the strength of interactions with $\alpha1^{Q-26'E}$, even though we predict a majority of $\alpha1$-β subunit interfaces in heteromeric GlyRs (26, 27). Interactions between the −26′ and 24′ side groups in both subunits were weaker, but not negligible in the $\alpha1$ subunit. The especially weak interaction energy between $\alpha1^{Q-26'}$ and $\beta^{K24'}$ supports the notion that the TZ of the β subunit is of lesser significance in receptor activation than the $\alpha1$ subunit.

Generality of −26′, 19′, and 24′ Interactions Across the pLGIC Family—In recent years high-resolution structures of several members of the pLGIC family in putative current conducting and non-conducting states have become available. These include different species of prokaryotic (15, 17–19) and

FIGURE 4. **Mutations to 24′.** *A*, $\alpha1^{K24'C}$ homomeric receptors show evidence of cysteine-cysteine cross-linking. A ~4 min application the reducing agent DTT (4 mM) resulted in a change in channel activity from infrequent, simple openings to more complex and wild-type-like activations. *B*, open dwell histograms for the corresponding recordings showing that before DTT the data are fit to a single exponential histogram, whereas after DTT the data are fit to multiple components. *C*, homomeric $\alpha1^{K24'A}$ receptors show a reduction in mean cluster duration and an increase in the intracluster shutting frequency. When $\alpha1^{K24'A}$ is combined with $\alpha1^{Q-26'E}$ in the same subunit ($\alpha1^{K24'A/Q-26'E}$), the resulting activations resemble those of the $\alpha1^{Q-26'E}$ homomers, but with reduced cluster durations. *D*, heteromeric $\alpha1\beta^{K24'A}$ and $\alpha1^{Q-26'E}$-$\beta^{K24'A}$ receptor activations suggest little effect of the $\beta^{K24'A}$ mutation. Bar graphs summarizing the effects on channel conductance, mean cluster duration, and intracluster shutting frequency for homomeric (*E*) and heteromeric (*F*) receptors incorporating 24′ mutations. The number of clusters used for homomeric receptors was 124 ($\alpha1^{K24'A}$, 4 patches) and 69 ($\alpha1^{Q-26'E/K24'A}$, 8 patches) and for heteromeric receptors was 114 ($\alpha1\beta^{K24'A}$, 7 patches) and 76 ($\alpha1^{Q-26'E}$-$\beta^{K24'A}$, 9 patches). ***, $p < 0.0001$; **, $p < 0.001$; *, $p < 0.01$.

TABLE 2
Pairwise coupling energies between $\alpha1^{Q-26'E}$ and 19′ or 24′ positions in $\alpha1$ and β subunits

	Θ parameter[a]	$\alpha1^{Q-26'E}$-$\alpha1^{R19'A}$	$\alpha1^{Q-26'E}$-$\alpha1^{K24'A}$	$\alpha1^{Q-26'E}$-$\beta^{A19'R}$	$\alpha1^{Q-26'E}$-$\beta^{K24'A}$
Pairwise coupling energy (kJ mol^{-1})	Clust. × Cond.	9.43	−0.97	1.60	−0.32
	Clust.	5.09	−1.06	1.06	−0.54
	Cond.	4.34	0.09	0.54	0.22
	Clust. × P_o	7.36	−3.84	1.09	−0.46
	MOC	4.68	−3.29	−1.08	1.17

[a] Clust., mean cluster duration (ms); Cond., conductance (pS); P_o, intracluster open state occupancy.

eukaryotic (14, 16, 20, 21) pLGICs. Given that these structures are static representations obtained under non-physiological conditions, it is vital to check them against functional data to ascertain if the crystal structures correspond to functionally relevant states. It is also useful to determine whether the putative interactions identified here are likely to have universal relevance across the pLGIC family. A structural alignment of two GLIC structures, in open (18) and closed (19) states (Fig. 6, *A* and *B*) reveals relative movements of the residues at −26′, 19′, and 24′ during channel opening.

To determine whether the interactions examined in this study represent a universal structural principal of pLGIC activation we measured the α-carbon-α-carbon (αC-αC) distances between the −26′ and 19′ positions and the −26′ and 24′ positions (Fig. 6*C*) in crystal structures of pLGICs in putative conducting and non-conducting configurations (Fig. 6*D*). Inclusion of structures in either the open-like or closed-like groups was based on a consideration of several features of each structure, including the minimum pore diameter, M2 orientation, and the molecules in which each receptor was co-crystalized. In each case, our classifications are in accord with those proposed by the original authors.

The residues at positions −26′ and 19′ have a significantly smaller mean αC-αC distance in conducting states (7.8 ± 0.1 Å) compared with nonconducting ones (12.9 ± 1.0 Å). The mean distance between positions −26′ and 24′ differs less between the two states, with a nonsignificant decrease from 12.9 ± 2.2 (nonconducting) to 9.7 ± 0.1 Å (conducting). The distances between −26′ and 19′, and −26′ and 24′ from a recently published GluCl structure in apo (closed) and POPC-bound confirmations (open) were excluded from the mean distance calculations (14). The decision to exclude these data were made on the basis that the αC-αC distances from −26′ to 19′ or 24′ were clear outliers, especially for −26′ to 19′. Furthermore, the POPC-bound (presumably open) structure differs from an earlier ivermectin- and glutamate-bound structure (16) in terms of the distances measured, and this earlier structure does conform to the general trends observed. This suggests that the apo and POPC-bound structures might not resemble physiological conformations, and so were excluded from further analysis.

Prediction of Synaptic Currents Mediated by $\alpha1^{Q-26'E}$-containing GlyRs—Finally, we investigated how the $\alpha1^{Q-26'E}$ hyperekplexia mutation might affect glycinergic inhibitory synaptic currents. Applying a saturating (1 mM) glycine concentration for brief periods (<1 ms) to outside-out membrane patches containing many receptors elicited synaptic-like ensemble currents. Wild-type α1 homomers and α1β heteromers activated rapidly, with 10–100% rise time constants of 0.24 ± 0.06 and 0.24 ± 0.02 ms, respectively. The decay time constants were also relatively brief, being 24.2 ± 7.3 ms for homomers and 15.7 ± 4.3 ms for heteromers (Fig. 7*A*). The β subunit had no significant influence on either parameter. Our results are consistent with those measured previously via similar techniques (36) and with synaptic currents of native synapses expressing α1 homomeric and α1β heteromeric GlyRs (37). This similarity in kinetics suggests that they are dominated by the α1 subunit. This inference was borne out in our experiments on $\alpha1^{Q-26'E}$ homomers and $\alpha1^{Q-26'E}$-β heteromers. Currents mediated by both receptors containing the $\alpha1^{Q-26'E}$ mutation were activated with rise time constants that were similar to wild-type receptors. These were 0.26 ± 0.03 and 0.31 ± 0.09 ms for homo- and heteromeric receptors, respectively. The decay time constants measured from $\alpha1^{Q-26'E}$ and $\alpha1^{Q-26'E}$-β receptors were an order of magnitude greater compared with their respective wild-type receptors (280 ± 41 and 272 ± 35 ms, respectively) and were not significantly different from each other (Fig. 7*A*).

It has been demonstrated that the time constant for deactivation of ensemble currents is the same as the burst durations at very low concentrations of ligand (38). However, it is difficult to predict what a sufficiently low concentration of glycine would be that might elicit burst durations that correspond to the measured decay times. We thus employed 2 μM glycine to activate bursts of activity from wild-type and $\alpha1^{Q-26'E}$-containing homomers and heteromers (Fig. 7*B*). 2 μM glycine induced bursts of activity in $\alpha1^{Q-26'E}$-containing receptors that were of longer duration compared with their wild-type counterparts. Wild-type α1 homomers were activated for a mean of 37 ± 4 ms, whereas the mean burst duration of $\alpha1^{Q-26'E}$ homomeric receptors was 947 ± 141 ms. Wild-type heteromers had a mean burst duration of 40 ± 3 ms and heteromers incorporating the $\alpha1^{Q-26'E}$ mutation had a mean burst duration of 344 ± 87 ms. The mean burst durations and ensemble current decay times were plotted on the same set of axes to investigate any correlation between them (Fig. 7*C*). A closer correspondence between burst duration and decay times was observed for wild-type receptors, the former quantity being ~1.5–2.5-fold greater than the latter. For receptors containing the $\alpha1^{Q-26'E}$ mutation there was greater deviation between the burst duration and current decay times, especially for $\alpha1^{Q-26'E}$ homomers. We make the following inferences from these data. First, that current kinetics in homo- and heteromeric receptors are dominated by the α1 subunit. Second, that there is a strong correlation between the burst duration and the decay rate of ensemble currents. Third, that 2 μM glycine is likely too high a concentration to elicit bursts that are sufficiently brief to account for the current decay times, especially for mutant-containing receptors. Fourth, that synaptic currents *in vivo* mediated by GlyRs expressing the $\alpha1^{Q-26'E}$ mutation will decay dramatically more slowly than wild-type.

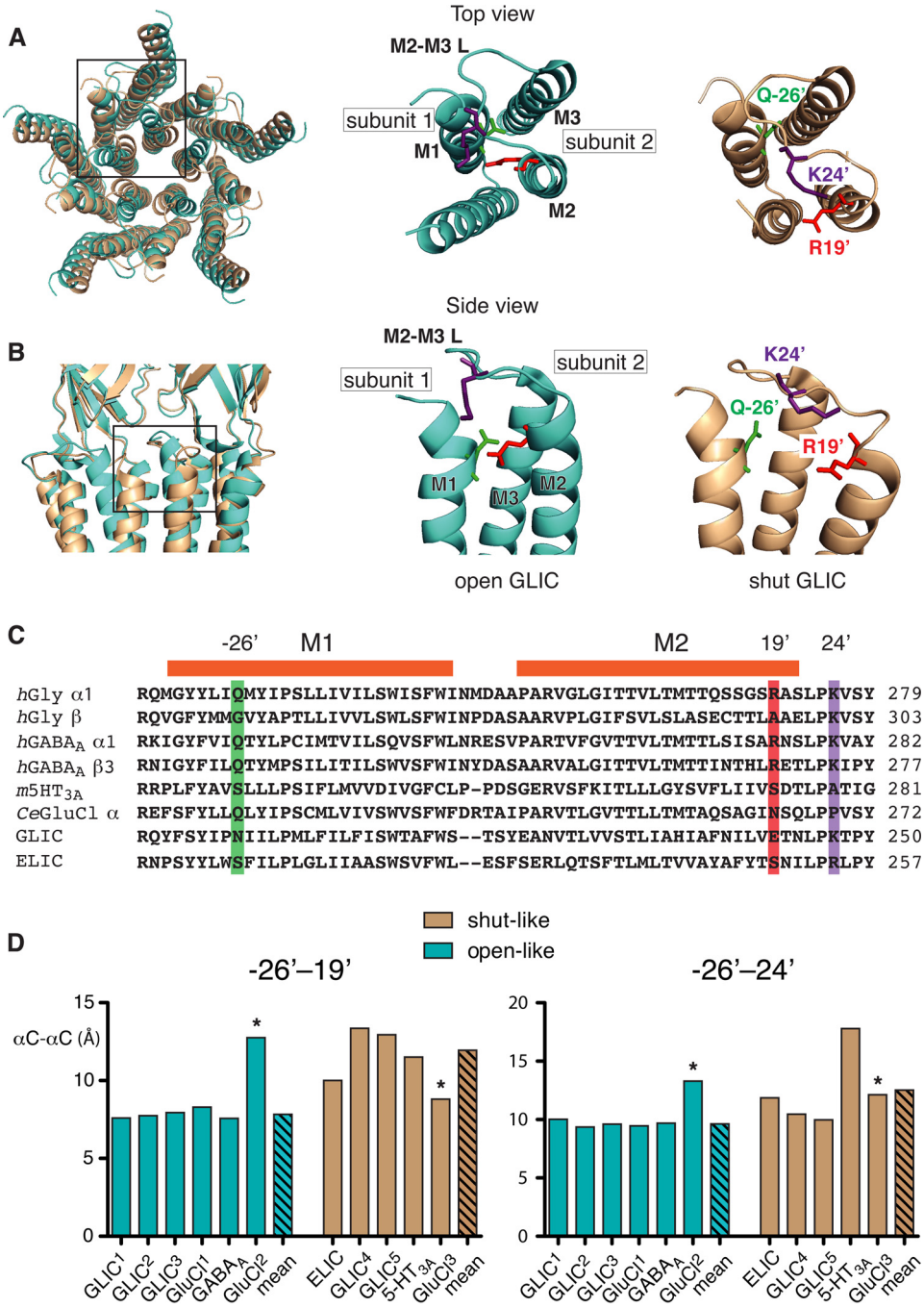

FIGURE 6. **Spatial relationship between −26′, 19′, and 24′ in pLGICs of known structure.** Superposition of top (*A*) and side (*B*) views of GLIC in putative open (*cyan*, Protein Data Bank code 3EHZ) and shut (*beige*, Protein Data Bank code 4NPQ) configurations showing the relative separation between positions, −26′, 19′, and 24′. *Boxed regions* showing the TDs of the open and shut structures with the first (M1) transmembrane domain of one subunit and the $Gln^{-26'}$ residue (*green*), and the second (M2) and third (M3) transmembrane domains of the adjacent subunit with $Arg^{19'}$ (*red*) and $Lys^{24'}$ (*purple*). The M2-M3 linker (M2-M3 L) is also shown. *C*, sequence alignment covering the region under investigation of selected pLGICs. Highlighted are the −26′, 19′, and 24′ positions. The prefixes on the sequence labels denote, human (*h*), mouse (*m*), and *Caenorhabditis elegans* (*Ce*). Included are the sequences of GLIC (*Gloeobacter violaceus*) and ELIC (*Erwinia chrysanthemi*). *D*, bar plots of the Cα-Cα distances between the −26′ and 19′ and −26′ and 24′ positions obtained from the indicated crystal structures. The measurements were taken from the following Protein Data Bank files, in parentheses, GLIC[1] (3EHZ), GLIC[2] (3EAM), GLIC[3] (3UU5), GLIC[4] (3UU3), GLIC[5] (4NPQ), ELIC (2VLO), GluCl[1] (3RIF), GluCl[2] (4TNW), GluCl[3] (4TNV), GABA$_A$ (4COF) and 5-HT$_{3A}$ (4PIR). *Asterisks* denote outlier values (GluCl[2] and GluCl[3]) that were omitted from the means.

DISCUSSION

Our aim was to investigate the mechanism by which the $\alpha 1^{Q-26'E}$ mutation induces spontaneous activity in homo- and heteromeric GlyRs on the level of single receptors. We reasoned that insights thus obtained may be used in conjunction with crystal structures of several, newly published pLCIC members to provide fundamental insights into the activation mechanisms of pLGICs in general. We investigated these receptors via single-channel analysis for two reasons. First, single channel kinetic analysis permits a quantitative understanding of the channel gating process and its underlying energetics (39, 40). Second, single channel conductance analysis allows us to deter-

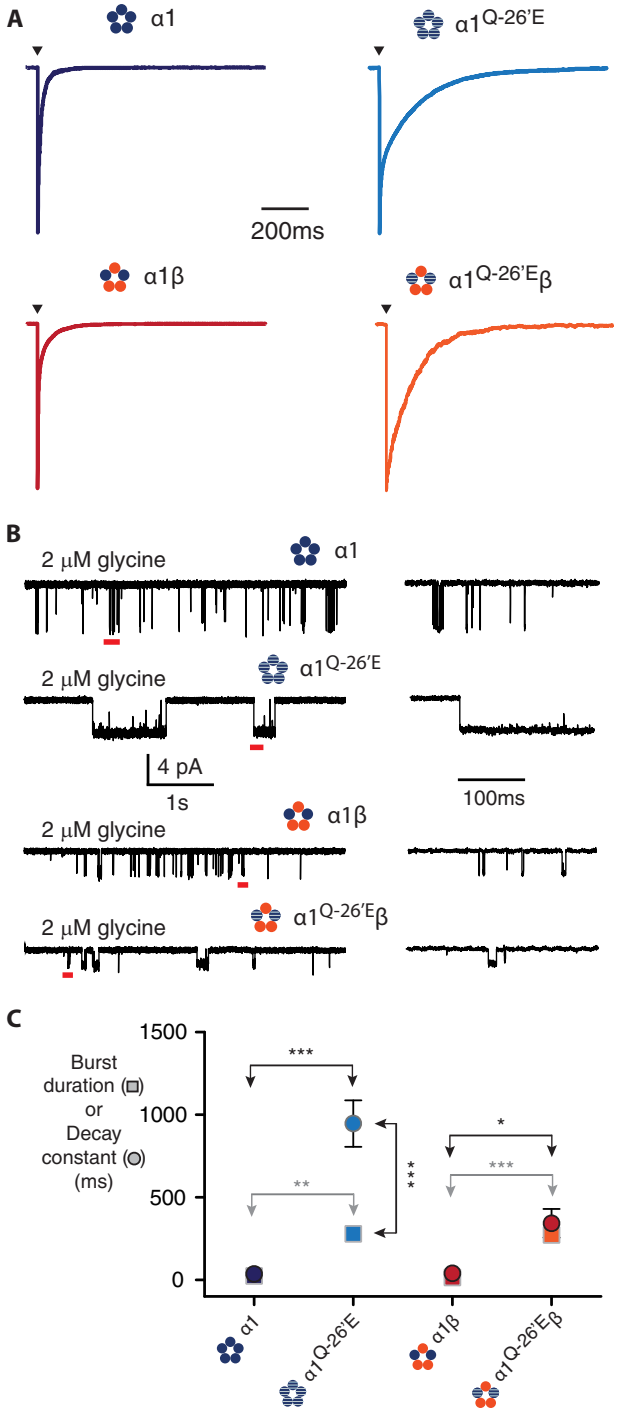

FIGURE 7. **Synaptic-like ensemble currents and burst durations in $\alpha1^{Q-26'E}$-containing homo- and heteromeric GlyRs.** *A*, sample ensemble currents recorded from outside-out patches containing the indicated receptors. The currents were elicited by brief (<1 ms) exposure to saturating (1 mM) glycine. Note the slower rates of current decay for currents mediated by $\alpha1^{Q-26'E}$-containing receptors. *B*, sample single channel recording in the presence of 2 μM glycine for the indicated receptors. The segments of record marked by a *red bar* are shown in expanded view on the *left*. *C*, mean values of burst duration (*circles*) and corresponding decay rates (*squares*) for the receptors in *A* and *B*. The number of bursts used in the analysis was 296 (α1 wild-type, 6 patches), 227 α1β (wild-type, 5 patches), 165 ($\alpha1^{Q-26'E}$, 7 patches), and 450 ($\alpha1^{Q-26'E}$-β, 5 patches). The number of patches used for the macropatch recordings was 5 (α1 wild-type), 9 α1β (wild-type), 11 ($\alpha1^{Q-26'E}$), and 3 ($\alpha1^{Q-26'E}$-β). ***, $p < 0.0001$; **, $p < 0.001$; *, $p < 0.01$.

mine whether mutations to residues near the pore lumen alter side group charge (24, 41). This would help us to resolve whether electrostatic interactions among the mutated residues affect receptor activation. The correlation between conductance and cluster length was critical for the interpretation of pairwise interactions because if a mutation did not affect conductance it also had no effect on cluster duration on receptors containing the $\alpha1^{Q-26'E}$ as a background. The importance of connecting cluster duration and conductance becomes clearer when comparing the $\alpha1^{Q-26'E/R19'A}$ receptors with $\alpha1^{Q-26'E/K24'A}$, $\alpha1^{Q-26'E}$-$\beta^{K24'A}$, or $\alpha1^{Q-26'E}$-$\beta^{A19'R}$ receptors. The $\alpha1^{R19'A}$ mutation decreases cluster duration and conductance on a wild-type background, and on an $\alpha1^{Q-26'E}$ background. In contrast, the $\alpha1^{K24'A}$ decreases cluster duration but not conductance. The $\alpha1^{Q-26'E/K24'A}$ double mutations had no additional effect on either parameter. The $\beta^{K24'A}$ or $\beta^{A19'R}$ mutations had no significant effects on cluster duration or conductance when co-expressed with either α1 wild-type or $\alpha1^{Q-26'E}$. These observations support the notion that $\alpha1^{K24'}$ is a salient gating element, but not as part of the $\alpha1^{Q-26'}$-$\alpha1^{R19'}$ pathway, whereas $\beta^{24'}$ or $\beta^{19'}$ positions seem not to support charge nor do they feature prominently in receptor activation.

Our finding that $\alpha1^{Q-26'E}$-β, $\alpha1^{Q-26'E}$-$\beta^{K24'A}$, and $\alpha1^{Q-26'E}$-$\beta^{A19'R}$ receptors are also spontaneously active in conjunction with high $\alpha1^{-26'}$-$\alpha1^{19'}$ coupling energy implies the presence of at least one α1-α1 interface. The stoichiometry of α1β GlyRs is in dispute, with some studies finding evidence for a 3α:2β ratio (42, 43) and others for a 2α:3β ratio (26, 27). If α and β subunits alternate in the pentamer, as proposed by both the Grudzinska and Yang studies (26, 27), the presence of at least one α1-α1 interface necessitates a 3α:2β ratio. This in turn implies that a single $\alpha1^{-26'}$-$\alpha1^{19'}$ electrostatic bond per pentamer in $\alpha1^{Q-26'E}$-containing receptors is sufficient to induce spontaneous activity and enhance the duration of ligand-induced activations.

Assuming that the coupling energies calculated here reflect relative degrees of local conformational movements necessary for the receptor to transition between stable functional states, we can deduce the following about GlyR (and other pLGIC) activation. The TZ of the α1 subunit is the most mobile, especially the extracellular portions of M1, M2, and the M2-M3 linker, compared with the TZ of the β subunit. The mean increase in proximity between $\alpha1^{-26'}$ and $\alpha1^{19'}$, between putative non-conducting and conducting states derived from crystal structures is greatest (>5 Å, Fig. 6). So too, is the $\Delta\Delta G_{int}$ for this interaction in the α1 subunit (Fig. 5). The $\alpha1^{-26'}$-$\alpha1^{19'}$ coupling energy is well within the range for a significant interaction between residues in pLGICs during activation (39, 40, 44) and between ligand binding residues and ligand (45). We propose that this interaction represents one point of energy transfer along what is likely to be a broad reaction coordinate (broad corrugated activation barrier) as proposed by Auerbach for the related nAChR (40, 46).

The cross-linking evidence suggests that the α1 M2-M3 linker is also highly mobile. This mobility is evidently necessary to produce activations that exhibit the type of complexity (multiple dwell components, Fig. 4) characteristic of wild-type receptors (12, 47). However, the mean change in separation

between $-26'$ and $24'$ between conducting and non-conducting states is less than that for $-26'$ and $19'$ (~3 Å), and the absolute distance between these two positions is greater (Fig. 6). The relatively low coupling energy associated with $\alpha1^{-26'}$ and $\alpha1^{24'}$, along with evidence that $\alpha1^{24'}$ mutations lead to profound perturbations in receptor activation suggests that this residue (and likely the M2-M3 linker) is involved in a different route of energy transfer to that of $\alpha1^{-26'}$ and $\alpha1^{19'}$. The $\alpha1^{K24'}$ may interact with aromatic residues in the β10-M1 linker (Fig. 1*A*, *inset*) to form cation-π contacts, as predicted by the crystal structure of the β3 homomeric $GABA_A$ receptor (21).

The coupling energies calculated for $\alpha1^{-26'}$ with $\beta^{19'}$ and $\beta^{24'}$ parallel those for the α1 subunit alone. However, the corresponding values suggest either weak or no interactions. This is reconcilable with the notion that the β subunit has a subordinate role in receptor activation (34). Moreover, adding a basic residue at $\beta^{19'}$ or removing one from $\beta^{24'}$ had little or no effect on channel conductance, respectively. These data suggest that the microenvironment around these positions is such that basic residues are weakly protonated (24), or otherwise not felt by permeating ions. $\beta^{24'}$-$\beta^{24'}$ cysteine cross-linking is not amenable to electrophysiology, but an $\alpha1^{-26'}$-$\beta^{24'}$ coupling energy that is comparable with the thermal energy of the receptor (40) would imply the βM2-M3 linker is relatively static with respect to $\alpha1^{-26'}$ during receptor activation. Together, these findings imply that many parts of the receptor change energy during activation.

We have demonstrated that the increased duration of unliganded (spontaneous) activity was paralleled by an increase in the durations of fully liganded activity (clusters) in receptors containing the $\alpha1^{Q-26'E}$ mutation. This is also the case for wild-type receptors. From this observation we infer that the $\alpha1^{Q-26'E}$ mutation has not uncoupled the activation mechanism as it occurs in wild-type receptors, allowing the transmembrane domains to adopt open, conducting conformation(s) by autonomously interacting with $\alpha1^{R19'}$. The indistinguishable conductance levels between unliganded and fully liganded receptors lend support to this inference (48, 49). Furthermore, we infer that by enhancing the $\alpha1^{-26'}$-$\alpha1^{19'}$ interaction, the $\alpha1^{Q-26'E}$ mutation has exposed a salient component of the activation mechanism of the wild-type receptor. If we assume that the receptors are in thermodynamic equilibrium, and that the ligand binding properties of receptors mutated at the TZ are little changed relative to wild-type (12, 50), then it follows that for an increase in the activation equilibrium constant for unliganded activation (an index of the efficacy with which the receptor transitions from non-conducting to conducting configurations) there will be a corresponding increase in the fully liganded activation equilibrium constant. This result has been well documented for constitutively active muscle nAChRs that bear mutations within the TZ (49, 51).

In summary, we sought to quantitate the strength of interactions between the $19'$, $24'$, and $-26'$ positions in contributing to the activation mechanism of both homo- and heteromeric GlyRs. We conclude that the $\alpha1^{-26'}$-$\alpha1^{19'}$ interaction is likely part of a significant pathway that distributes the energy of ligand binding to receptor activation. The significance of the interaction was made evident by the discovery that a single electrostatic interaction per $\alpha1^{Q-26'E}$-containing pentamer is sufficient to enhance receptor activation. The $24'$ position, although situated on a segment that is also highly mobile, is likely involved in a different energetic pathway. The local movements associated with these energetic interactions are evident in published crystal structures, indicating that they may pertain widely across the pLGIC family.

REFERENCES

1. Grosman, C., Zhou, M., and Auerbach, A. (2000) Mapping the conformational wave of acetylcholine receptor channel gating. *Nature* **403,** 773–776
2. Purohit, P., Gupta, S., Jadey, S., and Auerbach, A. (2013) Functional anatomy of an allosteric protein. *Nat. Commun.* **4,** 2984
3. Jha, A., Cadugan, D. J., Purohit, P., and Auerbach, A. (2007) Acetylcholine receptor gating at extracellular transmembrane domain interface: the Cys-loop and M2-M3 linker. *J. Gen. Physiol.* **130,** 547–558
4. Kash, T. L., Jenkins, A., Kelley, J. C., Trudell, J. R., and Harrison, N. L. (2003) Coupling of agonist binding to channel gating in the GABA(A) receptor. *Nature* **421,** 272–275
5. Lynch, J. W., Rajendra, S., Pierce, K. D., Handford, C. A., Barry, P. H., and Schofield, P. R. (1997) Identification of intracellular and extracellular domains mediating signal transduction in the inhibitory glycine receptor chloride channel. *EMBO J.* **16,** 110–120
6. Dreissen, Y. E., and Tijssen, M. A. (2012) The startle syndromes: physiology and treatment. *Epilepsia* **53,** 3–11
7. Bode, A., and Lynch, J. W. (2014) The impact of human hyperekplexia mutations on glycine receptor structure and function. *Mol. Brain* **7,** 2
8. Lynch, J. W. (2004) Molecular structure and function of the glycine receptor chloride channel. *Physiol. Rev.* **84,** 1051–1095
9. Langosch, D., Laube, B., Rundström, N., Schmieden, V., Bormann, J., and Betz, H. (1994) Decreased agonist affinity and chloride conductance of mutant glycine receptors associated with human hereditary hyperekplexia. *EMBO J.* **13,** 4223–4228
10. Rajendra, S., Lynch, J. W., Pierce, K. D., French, C. R., Barry, P. H., and Schofield, P. R. (1995) Mutation of an arginine residue in the human glycine receptor transforms β-alanine and taurine from agonists into competitive antagonists. *Neuron* **14,** 169–175
11. Lape, R., Plested, A. J., Moroni, M., Colquhoun, D., and Sivilotti, L. G. (2012) The α1K276E startle disease mutation reveals multiple intermediate states in the gating of glycine receptors. *J. Neurosci.* **32,** 1336–1352
12. Lewis, T. M., Sivilotti, L. G., Colquhoun, D., Gardiner, R. M., Schoepfer, R., and Rees, M. (1998) Properties of human glycine receptors containing the hyperekplexia mutation α1(K276E), expressed in *Xenopus* oocytes. *J. Physiol.* **507**, 25–40
13. Bode, A., Wood, S. E., Mullins, J. G., Keramidas, A., Cushion, T. D., Thomas, R. H., Pickrell, W. O., Drew, C. J., Masri, A., Jones, E. A., Vassallo, G., Born, A. P., Alehan, F., Aharoni, S., Bannasch, G., Bartsch, M., Kara, B., Krause, A., Karam, E. G., Matta, S., Jain, V., Mandel, H., Freilinger, M., Graham, G. E., Hobson, E., Chatfield, S., Vincent-Delorme, C., Rahme, J. E., Afawi, Z., Berkovic, S. F., Howell, O. W., Vanbellinghen, J. F., Rees, M. I., Chung, S. K., and Lynch, J. W. (2013) New hyperekplexia mutations provide insight into glycine receptor assembly, trafficking, and activation mechanisms. *J. Biol. Chem.* **288,** 33745–33759
14. Althoff, T., Hibbs, R. E., Banerjee, S., and Gouaux, E. (2014) X-ray structures of GluCl in apo states reveal a gating mechanism of Cys-loop receptors. *Nature* **512,** 333–337
15. Bocquet, N., Nury, H., Baaden, M., Le Poupon, C., Changeux, J. P., Delarue, M., and Corringer, P. J. (2009) X-ray structure of a pentameric ligand-gated ion channel in an apparently open conformation. *Nature* **457,** 111–114
16. Hibbs, R. E., and Gouaux, E. (2011) Principles of activation and permeation in an anion-selective Cys-loop receptor. *Nature* **474,** 54–60
17. Hilf, R. J., and Dutzler, R. (2008) X-ray structure of a prokaryotic pentameric ligand-gated ion channel. *Nature* **452,** 375–379
18. Hilf, R. J., and Dutzler, R. (2009) Structure of a potentially open state of a proton-activated pentameric ligand-gated ion channel. *Nature* **457,**

115–118
19. Sauguet, L., Shahsavar, A., Poitevin, F., Huon, C., Menny, A., Nemecz, À., Haouz, A., Changeux, J. P., Corringer, P. J., and Delarue, M. (2014) Crystal structures of a pentameric ligand-gated ion channel provide a mechanism for activation. *Proc. Natl. Acad. Sci. U.S.A.* **111,** 966–971
20. Hassaine, G., Deluz, C., Grasso, L., Wyss, R., Tol, M. B., Hovius, R., Graff, A., Stahlberg, H., Tomizaki, T., Desmyter, A., Moreau, C., Li, X. D., Poitevin, F., Vogel, H., and Nury, H. (2014) X-ray structure of the mouse serotonin 5-HT3 receptor. *Nature* **512,** 276–281
21. Miller, P. S., and Aricescu, A. R. (2014) Crystal structure of a human GABAA receptor. *Nature* **512,** 270–275
22. Bode, A., and Lynch, J. W. (2013) Analysis of hyperekplexia mutations identifies transmembrane domain rearrangements that mediate glycine receptor activation. *J. Biol. Chem.* **288,** 33760–33771
23. Cymes, G. D., and Grosman, C. (2008) Pore-opening mechanism of the nicotinic acetylcholine receptor evinced by proton transfer. *Nat. Struct. Mol. Biol.* **15,** 389–396
24. Cymes, G. D., Ni, Y., and Grosman, C. (2005) Probing ion-channel pores one proton at a time. *Nature* **438,** 975–980
25. Groot-Kormelink, P. J., Beato, M., Finotti, C., Harvey, R. J., and Sivilotti, L. G. (2002) Achieving optimal expression for single channel recording: a plasmid ratio approach to the expression of α1 glycine receptors in HEK293 cells. *J. Neurosci. Methods* **113,** 207–214
26. Yang, Z., Taran, E., Webb, T. I., and Lynch, J. W. (2012) Stoichiometry and subunit arrangement of $\alpha1\beta$ glycine receptors as determined by atomic force microscopy. *Biochemistry* **51,** 5229–5231
27. Grudzinska, J., Schemm, R., Haeger, S., Nicke, A., Schmalzing, G., Betz, H., and Laube, B. (2005) The β subunit determines the ligand binding properties of synaptic glycine receptors. *Neuron* **45,** 727–739
28. Barry, P. H. (1994) JPCalc, a software package for calculating liquid junction potential corrections in patch-clamp, intracellular, epithelial and bilayer measurements and for correcting junction potential measurements. *J. Neurosci. Methods* **51,** 107–116
29. Qin, F. (2004) Restoration of single-channel currents using the segmental *k*-means method based on hidden Markov modeling. *Biophys. J.* **86,** 1488–1501
30. Qin, F., Auerbach, A., and Sachs, F. (1997) Maximum likelihood estimation of aggregated Markov processes. *Proc. Biol. Sci.* **264,** 375–383
31. Sivilotti, L. G. (2010) What single-channel analysis tells us of the activation mechanism of ligand-gated channels: the case of the glycine receptor. *J. Physiol.* **588,** 45–58
32. Bormann, J., Rundström, N., Betz, H., and Langosch, D. (1993) Residues within transmembrane segment M2 determine chloride conductance of glycine receptor homo- and hetero-oligomers. *EMBO J.* **12,** 3729–3737
33. Moorhouse, A. J., Jacques, P., Barry, P. H., and Schofield, P. R. (1999) The startle disease mutation Q266H, in the second transmembrane domain of the human glycine receptor, impairs channel gating. *Mol. Pharmacol.* **55,** 386–395
34. Shan, Q., Nevin, S. T., Haddrill, J. L., and Lynch, J. W. (2003) Asymmetric contribution of α and β subunits to the activation of $\alpha\beta$ heteromeric glycine receptors. *J. Neurochem.* **86,** 498–507
35. Lynch, J. W., Han, N. L., Haddrill, J., Pierce, K. D., and Schofield, P. R. (2001) The surface accessibility of the glycine receptor M2-M3 loop is increased in the channel open state. *J. Neurosci.* **21,** 2589–2599
36. Mohammadi, B., Krampfl, K., Cetinkaya, C., Moschref, H., Grosskreutz, J., Dengler, R., and Bufler, J. (2003) Kinetic analysis of recombinant mammalian $\alpha(1)$ and $\alpha(1)\beta$ glycine receptor channels. *Eur. Biophys. J.* **32,** 529–536
37. Legendre, P. (1997) Pharmacological evidence for two types of postsynaptic glycinergic receptors on the Mauthner cell of 52-h-old zebrafish larvae. *J. Neurophysiol.* **77,** 2400–2415
38. Wyllie, D. J., Béhé, P., and Colquhoun, D. (1998) Single-channel activations and concentration jumps: comparison of recombinant NR1a/NR2A and NR1a/NR2D NMDA receptors. *J. Physiol.* **510**, 1–18
39. Auerbach, A. (2013) The energy and work of a ligand-gated ion channel. *J. Mol. Biol.* **425,** 1461–1475
40. Auerbach, A. (2010) The gating isomerization of neuromuscular acetylcholine receptors. *J. Physiol.* **588,** 573–586
41. Keramidas, A., Moorhouse, A. J., Schofield, P. R., and Barry, P. H. (2004) Ligand-gated ion channels: mechanisms underlying ion selectivity. *Prog. Biophys. Mol. Biol.* **86,** 161–204
42. Durisic, N., Godin, A. G., Wever, C. M., Heyes, C. D., Lakadamyali, M., and Dent, J. A. (2012) Stoichiometry of the human glycine receptor revealed by direct subunit counting. *J. Neurosci.* **32,** 12915–12920
43. Langosch, D., Thomas, L., and Betz, H. (1988) Conserved quaternary structure of ligand-gated ion channels: the postsynaptic glycine receptor is a pentamer. *Proc. Natl. Acad. Sci. U.S.A.* **85,** 7394–7398
44. Cadugan, D. J., and Auerbach, A. (2010) Linking the acetylcholine receptor-channel agonist-binding sites with the gate. *Biophys. J.* **99,** 798–807
45. Purohit, P., Bruhova, I., Gupta, S., and Auerbach, A. (2014) Catch-and-hold activation of muscle acetylcholine receptors having transmitter binding site mutations. *Biophys. J.* **107,** 88–99
46. Auerbach, A. (2005) Gating of acetylcholine receptor channels: brownian motion across a broad transition state. *Proc. Natl. Acad. Sci. U.S.A.* **102,** 1408–1412
47. Burzomato, V., Beato, M., Groot-Kormelink, P. J., Colquhoun, D., and Sivilotti, L. G. (2004) Single-channel behavior of heteromeric $\alpha1\beta$ glycine receptors: an attempt to detect a conformational change before the channel opens. *J. Neurosci.* **24,** 10924–10940
48. Jackson, M. B. (1984) Spontaneous openings of the acetylcholine receptor channel. *Proc. Natl. Acad. Sci. U.S.A.* **81,** 3901–3904
49. Purohit, P., and Auerbach, A. (2009) Unliganded gating of acetylcholine receptor channels. *Proc. Natl. Acad. Sci. U.S.A.* **106,** 115–120
50. Grosman, C., Salamone, F. N., Sine, S. M., and Auerbach, A. (2000) The extracellular linker of muscle acetylcholine receptor channels is a gating control element. *J. Gen. Physiol.* **116,** 327–340
51. Grosman, C., and Auerbach, A. (2000) Kinetic, mechanistic, and structural aspects of unliganded gating of acetylcholine receptor channels: a single-channel study of second transmembrane segment 12′ mutants. *J. Gen. Physiol.* **115,** 621–635